Available online at www.sciencedirect.com
ScienceDirect
Ceramics International 34 (2008) 1885–1892
CERAMICS INTERNATIONAL
www.elsevier.com/locate/ceramint

# Sintering of tricalcium phosphate–fluorapatite composites by addition of alumina

Foued Ben Ayed [a,b,*], Jamel Bouaziz [a]

[a] *Laboratoire de Chimie Industrielle, Ecole Nationale d'Ingénieurs de Sfax, BP W, 3038 Sfax, Tunisia*
[b] *Institut Préparatoire aux Etudes d'Ingénieurs de Sfax, BP 805, 3018 Sfax, Tunisia*

Received 9 May 2007; received in revised form 10 June 2007; accepted 1 July 2007
Available online 15 August 2007

**Abstract**

The effect of alumina ($Al_2O_3$) addition on the densification of tricalcium phosphate–26.52 wt% fluorapatite composites was investigated. The sintering behaviour was investigated using X-ray diffraction, scanning electron microscopy and by analysis using $^{31}P$ and $^{27}Al$ nuclear magnetic resonance. The composites sintering alumina additives have been tested in order to enhance their sinterability. When small amount of $Al_2O_3$ was added, densification of the tricalcium phosphate–26.52 wt% fluorapatite composites was markedly enhanced. The densification of the pure tricalcium phosphate–26.52 wt% fluorapatite composites was about 87%, whereas it reached 91% with 2.5 wt% $Al_2O_3$ at 1300 °C. High temperatures were not very efficient conditions. About 1400 °C, grain growth becomes important and induces an intragranular porosity which is responsible for decrease in density. The $^{31}P$ and $^{27}Al$ MAS-NMR analysis of tricalcium phosphate–26.52 wt% fluorapatite composites sintered with $Al_2O_3$ additives reveals the presence of tetrahedral P and octahedral Al sites.


*Keywords:* A. Sintering; B. Composites; B. Porosity; D. $Al_2O_3$; Bioceramics

## 1. Introduction

Calcium phosphates constitute an important family of bioceramics resembling the part of calcified tissues, particularly hydroxyapatite $Ca_{10}(PO_4)_6(OH)_2$ (Hap), tricalcium phosphate $Ca_3(PO_4)_2$ (TCP) and fluorapatite $Ca_{10}(PO_4)_6F_2$ (Fap) [1–16]. Most studies have been reported on the sintering behaviour and mechanical proprieties of TCP–Hap composites [3–7,15,16]. On the contrary little work has been devoted on the sintering of TCP–Fap composites [17]. But the majority of bioceramics have a low density which decrease the mechanical properties. However, TCP and Hap have poor mechanical resistance [3–7]. In this study, Fap has been used with a fixed 26.52 wt% amount because the human bone contains 1 wt% of fluorine approximately [18]. In fact, Fap possesses a potential advantage over Hap with its higher chemical stability and aptitude to delay caries' process without the biocompatibility degradation [5]. It is known that the fluorine ion itself protects dental caries and also enhances mineralization and crystallization [19]. Fap has shown good phase stability even at higher temperature [8,9,14]. Hence, ceramic oxides or metallic dispersions have been introduced as reinforcing agents [20–22]. Among the ceramic reinforcements, alumina ($Al_2O_3$) has been used in orthopaedic applications due to its excellent wear resistance. This study deals to produce biphasic calcium phosphate (TCP–Fap) composites sintering at different temperatures between 1100 °C and 1400 °C and with various $Al_2O_3$ additives amounts (2.5 wt%, 5 wt%, 10 wt% and 20 wt%).

## 2. Preparation, materials and methods

The TCP powder was synthesised by solid state reaction [23]. The calcium carbonate ($CaCO_3$, Merck) was added to diammonium hydrogenophosphate ($(NH_4)_2HPO_4$, Merck) at 900 °C, according to the following reaction:

$$3CaCO_3 + 2(NH_4)_2HPO_4 \rightarrow Ca_3(PO_4)_2 + 3CO_2 + 4NH_3 + 3H_2O \quad (1)$$

The phenolphthalein test was used to detect CaO. The reaction finish was indicated by CaO absence.

* Corresponding author. Tel.: +216 98 252 033; fax: +216 74 275 595.
*E-mail address:* benayedfoued@yahoo.fr (F.B. Ayed).

0272-8842/$34.00 
doi:10.1016/j.ceramint.2007.07.017

Fap powder is synthesised by precipitation method [9]. A calcium nitrate ($Ca(NO_3)\cdot 4H_2O$, Merck) solution was slowly added to a boiling solution containing diammonium hydrogenophosphate ($(NH_4)_2HPO_4$, Merck) and ammonium fluoride ($NH_4F$, Merck), with continuous magnetic stirring. During the reaction, pH was adjusted to the same level (pH 8–9) by adding ammonia. The obtained precipitate was filtered and washed with deionised water; it is then dried at 70 °C for 12 h. The specific surface area (SSA) of powder was measured by nitrogen absorption from the BET method (ASAP 200) [24]. The primary particle size ($D_{BET}$) was calculated by assuming the primary particles to be spherical [9]:

$$D_{BET} = \frac{6}{S\rho} \quad (2)$$

where $\rho$ is the theoretical density of Fap (3.19 g/cm$^3$) and TCP (3.07 g/cm$^3$), and $S$ is the specific surface area of powder.

The X-ray diffraction pattern of sintered pieces was obtained by a Seifert XRD 3000 TT diffractometer (monochromatized Cu Kα radiation) and compared with the JCPDS files. The obtained products were examined by scanning electron microscope (SEM) (Philips XL 30). The CaO included in the powder was determined by phenolphthalein test (Afnor S94-066). Differential thermal analysis was carried out using about 30 mg of powder (DTA; Model Setaram) with heating rate about 5 °C min$^{-1}$. The TCP–Fap composites were characterized by high resolution solid state MAS-NMR using a BRUKER 300WB spectrometer. NMR spectra were recorded at a $^{31}P$ frequency of 121.5 MHz (field of 7.04 T) and $^{27}Al$ frequency of 78.2 MHz (field of 7.04 T). Approximately 50 mg of samples was used. The $^{31}P$ NMR chemical shifts reference is the phosphoric acid. The $^{27}Al$ NMR chemical shifts were referenced to a static signal obtained from an aqueous aluminium chloride solution.

The TCP–26.52 wt% Fap composites and $Al_2O_3$ additive (Merck) were mixed in an agate mortar. The $Al_2O_3$ powder was used in all experiments with average grain size about 3 μm (Table 1). The powder mixtures were milled in ethanol with high-purity $Al_2O_3$ balls as media for 24 h. After milling, the mixtures were dried in a rotary vacuum evaporator and passed through a 70-mesh screen. After drying at 80 °C for 24 h, the powder mixtures were moulded in a cylinder having a 13 mm diameter and 4 mm thickness and pressed under 150 MPa. The green compacts were sintered in a super khantal furnace with $Al_2O_3$ additive at various temperatures (1100–1400 °C). The heating time was measured from the point at which the furnace reaches the heating temperature. The samples are held for different hold times. The best hold time for obtaining the densification maximum is 1 h. The heating rate was 10 °C min$^{-1}$. The bulk density of the sintered body was measured by geometrical measurement. Three tests were made for every experiment. The relative error of densification value was about 1%.

Table 1
SSA, average grain size obtained by different analysis and sintering temperature of various compounds

| Compound | SSA (m$^2$/g) ±1.00 | $D_{BET}$ (μm) ±0.20 | $D_{50}$ (μm) ±0.2[a] | $T$ (°C) |
|---|---|---|---|---|
| Fap [9] | 29.00 | 0.07 | 6 | 715 |
| TCP [23] | 1.13 | 1.73 | 9 | 1050 |
| Composites[b] | 1.20 | 1.60 | 11 | 1080 |
| $Al_2O_3$ | 2.87 | 0.53 | 3 | – |

[a] Mean diameter, $T$: sintering temperature.
[b] TCP–26.52 wt% Fap.

## 3. Results and discussion

### 3.1. Characterization of ceramics specimens

The SSA of Fap and TCP is 29 m$^2$/g and 1.13 m$^2$/g, respectively. The X-ray diffraction (XRD) pattern obtained from TCP powder reveals only peaks of TCP without any other structures (Fig. 1a). The phenolphthalein test was negative. But it must be kept in mind that XRD analysis does not detect the presence of a small amount of impurities, especially when compounds have poor crystallinity. The XRD pattern obtained from Fap calcined powder at 900 °C illustrated peaks relative of Fap and $CaF_2$ traces (Fig. 1b). At 1300 °C, only Fap crystalline phase in the material and a small amount of CaO are detected (Fig. 1c). The CaO traces formation revealed by XRD and phenolphthalein test shows the $CaF_2$ hydrolysis at this temperature [9].

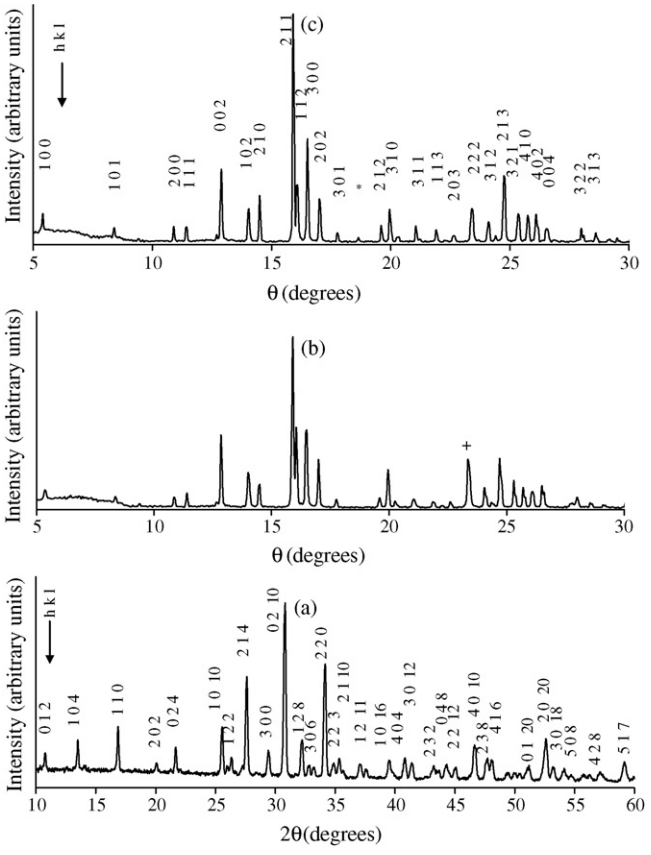


Fig. 1. XRD patterns for: (a) TCP powder calcined at 900 °C; (b) Fap powder calcined at 900 °C (+: $CaF_2$) and (c) Fap powder calcined at 1300 °C (*: CaO).

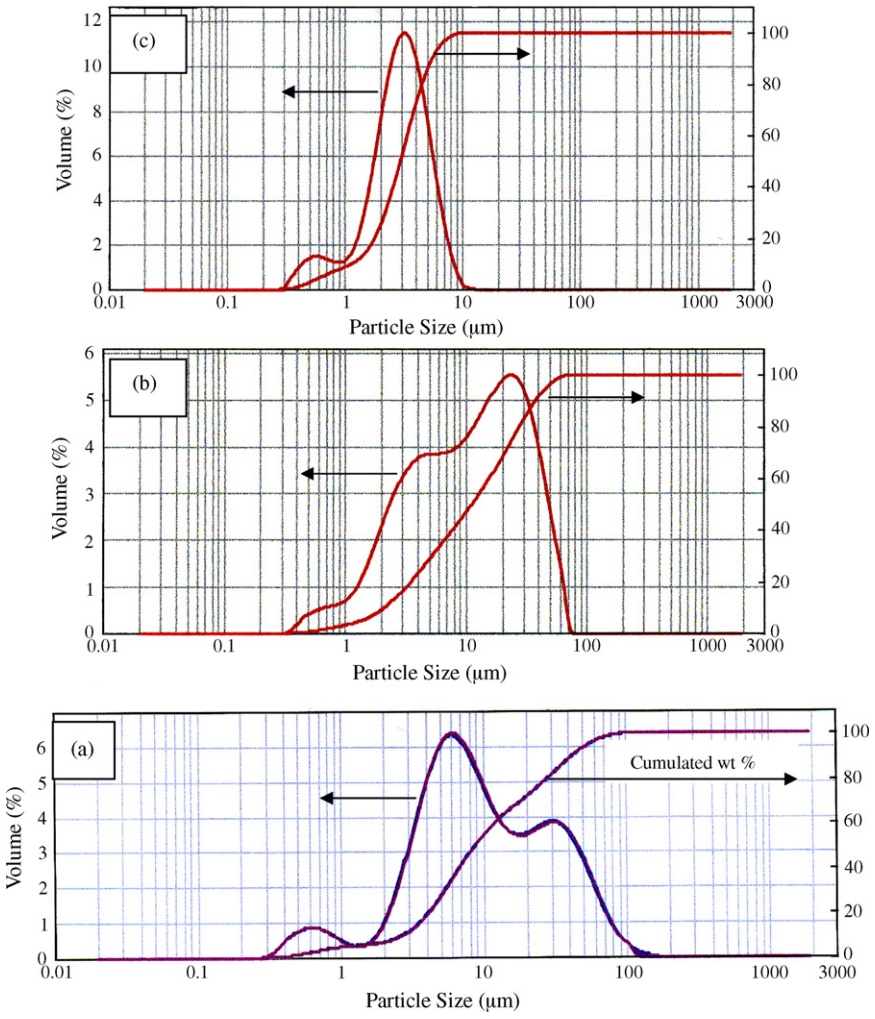


Fig. 2. Curves of granulometric repartition of: (a) TCP powder; (b) TCP–26.52 wt% Fap powder and (c) alumina.

The Fap and TCP particle are assumed to be spherical; the particle size can be calculated using Eq. (2). The results of average grain size obtained by SSA ($D_{BET}$) and average grain size obtained by granulometric repartition ($D_{50}$) are presented in Table 1. These values ($D_{BET}$) obtained by SSA do not correspond to those obtained from the particle size distribution (Fig. 2 and Table 1). The discrepancy may be due to the presence of agglomerates which are formed during calcinations. The dilatometric measurements of Fap, TCP and TCP–26.52 wt% Fap composites showed that shrinkage began at about 715 °C, 1050 °C and 1080 °C, respectively (Table 1) [9,23]. The addition of 26.52 wt% Fap in the matrix of TCP increases the sintering temperature of 30 °C in comparison with the pure TCP.

Typical DTA curve of Fap powder is given in Fig. 3a. Two endothermic peaks are observed in the DTA curve of Fap. The peak around 90 °C is due to the departure of adsorbed water. The second peak around 1180 °C may be due to the formation of a liquid phase, which is formed from binary eutectic between $CaF_2$ and Fap [8]. Fluorite ($CaF_2$) is assumed to be formed as a second phase during the powder preparation of Fap. Typical DTA curve of TCP powder illustrate two endothermic peaks (Fig. 3b). The first is located at 1285 °C, corresponding to the first allotropic transformation of the TCP (β → α). The second appearing at 1475 °C corresponds to the second allotropic transformation of the TCP (α → α′).

### 3.2. Sinterability of TCP–Fap composites

The experiment is carried out on some samples containing different wt% of $Al_2O_3$ (0 wt%, 2.5 wt%, 5 wt%, 10 wt% and 20 wt%) at various temperatures (1100 °C, 1200 °C, 1300 °C

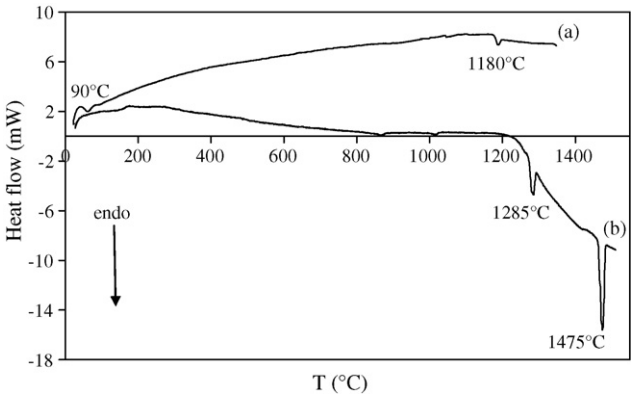


Fig. 3. DTA curves of: (a) Fap powder and (b) TCP powder.

Table 2
Apparent porosity vs. temperature of TCP–26.52 wt% Fap composites sintered with different wt% of $Al_2O_3$ for 1 h

| wt% $Al_2O_3$/$T$ (°C) | Apparent porosity ± 1 (%) | | | |
|---|---|---|---|---|
| | 1100 | 1200 | 1300 | 1400 |
| 0 | 30.0 | 17.2 | 13.0 | – |
| 2.5 | 32.8 | 18.8 | 9.0 | 12.4 |
| 5 | 33.8 | 21.0 | 11.0 | 13.1 |
| 10 | 35.8 | 24.5 | 18.1 | 19.0 |
| 20 | 39.0 | 27.5 | 20.8 | 21.6 |

and 1400 °C) (Table 2). Fig. 4 shows the results for apparent porosity of TCP–26.52 wt% Fap composites sintered for 1 h. The ultimate densification is attained at 1300 °C with 2.5 wt% $Al_2O_3$ (91%) and the minimum densification is approached at 1100 °C with 20 wt% $Al_2O_3$ (Table 2). When 2.5 wt% or 5 wt% $Al_2O_3$ are added, there was a considerable reduction in porosity for all temperatures, nearly 9% at 1300 °C. Above 10 wt% $Al_2O_3$, the relative density decreases with additive contents and the final density is always less than the value of the pure composites in the same condition. At 1400 °C and without alumina, it is impossible to determine their density because the samples are cooled in the support.

### 3.3. Characterization of sintered samples

After sintering, the samples have been characterized by different techniques: $^{31}P$ and $^{27}Al$ MAS-NMR, X-ray diffraction and scanning electronic microscopy.

Solid state magic angle spinning (MAS) nuclear magnetic resonance (NMR) spectroscopy has proven to be a powerful technique for analysing chemically active sites in solid materials. The evolution of the local environment of the aluminium and phosphorus atoms was followed during the sintering process by $^{27}Al$ and $^{31}P$ MAS-NMR. These experiments were implemented, both the assignments of phosphorus and aluminium sites and the quantification of their relative compositions in the composite. Therefore, $^{31}P$ and $^{27}Al$ MAS-NMR would be used to study the reactions and interactions between (TCP–Fap–$Al_2O_3$) system three solid phases.

The $^{31}P$ MAS-NMR spectra of TCP–26.52 wt% Fap composites sintered for 1 h at various temperatures (1100 °C, 1200 °C, 1300 °C and 1400 °C) without $Al_2O_3$ are presented in Fig. 5; which shows a broad peak (centred on 4.75 ppm) and an intense peak at 0.10 ppm; that is assigned to the phosphorus of three tetrahedral P sites relative of TCP. The same figure which illustrates an intense peak at 2.81 ppm relative to the phosphorus of Fap, is assigned to tetrahedral sites ($Q^1$). The $^{31}P$ MAS-NMR spectra of TCP illustrate three peaks (at 4.75 ppm, 0.10 ppm and 1.02 ppm). This result was confirmed by Yashima et al. [25]. Indeed, they show that the phosphorus atoms are located in three crystallographic sites of $P(1)O_4$, $P(2)O_4$ and $P(3)O_4$. In the $^{31}P$ MAS-NMR spectra of the composites, the peak relative of Fap increases with sintering temperature (1100–1400 °C) (the chemical shift (d) in Fig. 5). This can be attributed to the solid reaction between $CaF_2$ and

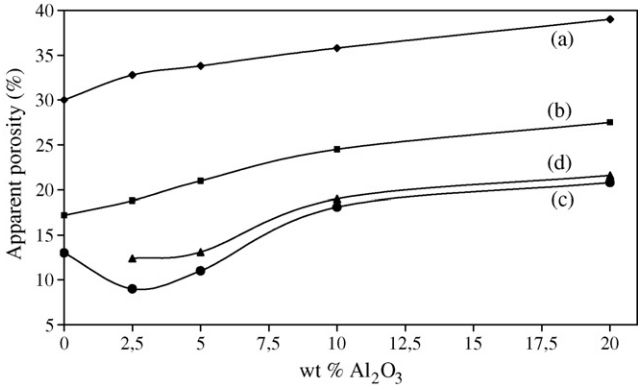


Fig. 4. Apparent porosity vs. temperature of TCP–26.52 wt% Fap composites sintered for 1 h with different wt% $Al_2O_3$ at: (a) 1100 °C; (b) 1200 °C; (c) 1300 °C and (d) 1400 °C.

TCP. $CaF_2$ exists in the initial powder of Fap [8,9]. Indeed, the curve of Fap TDA shows an endothermic peak at 1180 °C relative to an eutectic formed between Fap and $CaF_2$ [8,9]. The solid reaction of the new quantity of Fap is the following:

$$3Ca_3(PO_4)_{2(s)} + CaF_{2(s)} \rightarrow Ca_{10}(PO_4)_6F_{2(s)} \quad (3)$$

The $^{31}P$ MAS-NMR spectra of TCP–26.52 wt% Fap composites sintered for 1 h with 2.5 wt% $Al_2O_3$ at various temperatures (1100 °C, 1200 °C, 1300 °C and 1400 °C) are reported in Fig. 6b–e. The $^{31}P$ MAS-NMR spectra in the Fig. 6b–e are very similar to spectra in Fig. 5. Exceptionally, an intense peak at (−1.99 ppm) is assigned probably to $Ca_4(PO_4)_2O$ phase. This analysis reveals the presence of tetrahedral P sites (−1.99 ppm, −0.08 ppm, 2.76 ppm and 4.25 ppm) [25].

The $^{31}P$ MAS-NMR spectra of TCP–26.52 wt% Fap composites sintered for 1 h at 1300 °C with various wt% of $Al_2O_3$ (0 wt%, 2.5 wt% and 20 wt%) are presented in Fig. 6a, d and f. These spectra present the same structure practically, which show peaks relative to TCP (−0.08 ppm and 4.75 ppm),

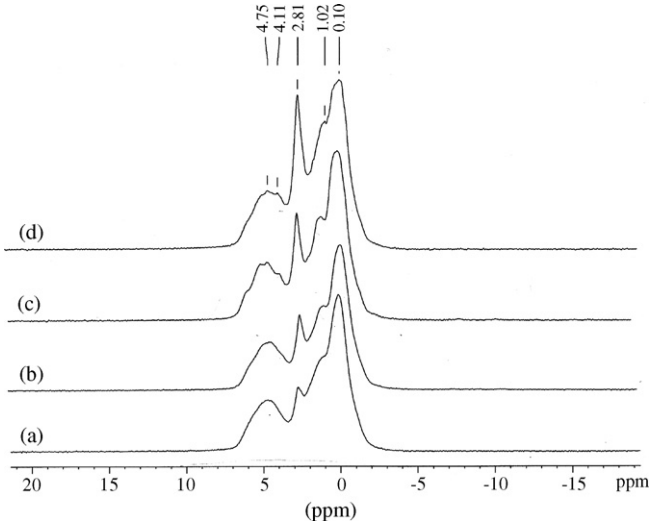


Fig. 5. $^{31}P$ NMR spectra of TCP–26.52 wt% Fap composites sintered without $Al_2O_3$ for 1 h at: (a) 1100 °C; (b) 1200 °C; (c) 1300 °C and (d) 1400 °C.

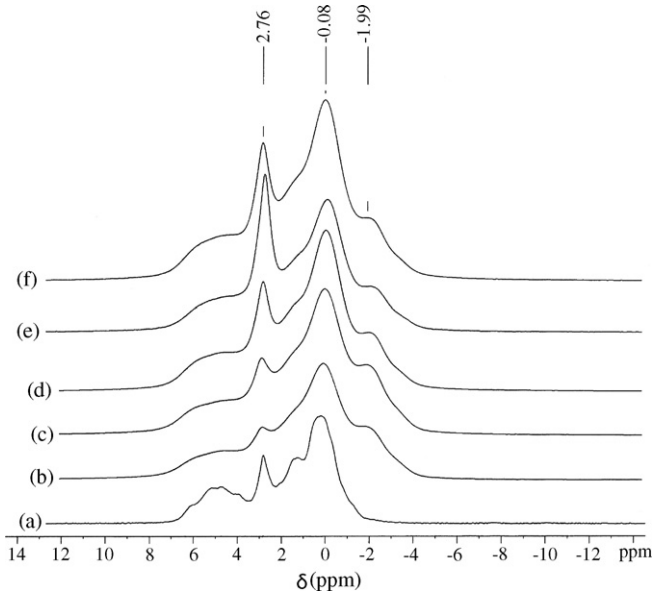


Fig. 6. $^{31}$P NMR spectra of TCP–26.52 wt% Fap composites sintered at various temperatures and with different wt% $Al_2O_3$ for 1 h: (a) 0 wt% $Al_2O_3$, 1300 °C; (b) 2.5 wt% $Al_2O_3$, 1100 °C; (c) 2.5 wt% $Al_2O_3$, 1200 °C; (d) 2.5 wt% $Al_2O_3$, 1300 °C; (e) 2.5 wt% $Al_2O_3$, 1400 °C and (f) 10 wt% $Al_2O_3$, 1300 °C.

relative to Fap (2.76 ppm) and a signal observed at 1400 °C around (−1.99 ppm) relative probably to $Ca_4(PO_4)_2O$ phase [26].

The $^{27}$Al MAS-NMR spectra of the TCP–26.52 wt% Fap composites sintered for 1 h at various temperatures (1100 °C, 1200 °C, 1300 °C and 1400 °C) with 2.5 wt% $Al_2O_3$ reveal the presence of octahedral Al sites (−9.81 ppm) (Fig. 7a–d). The chemical shift shows the presence of Al–O bands. The intense peak around (−9.81 ppm) is assigned probably to $CaAl_2O_4$ phase [27]. The analysis by $^{27}$Al MAS-NMR for the TCP–26.52 wt% Fap composites sintered for 1 h at 1300 °C for different $Al_2O_3$ percentages (2.5 wt% and 10 wt%) (Fig. 7c and e) shows the same peak revealed in the Fig. 7a, b and d. Exceptionally, the $^{27}$Al MAS-NMR spectrum of composites sintered with 10 wt% $Al_2O_3$ illustrates the increase of the peak intensity relative to $Al_2O_3$ for the sample. The small signal detected around 6–15 and 39.23 ppm in Fig. 7e could be due to $Al_2O_3$ additives phase in the composites, which assigned the presence of tetrahedral and octahedral sites.

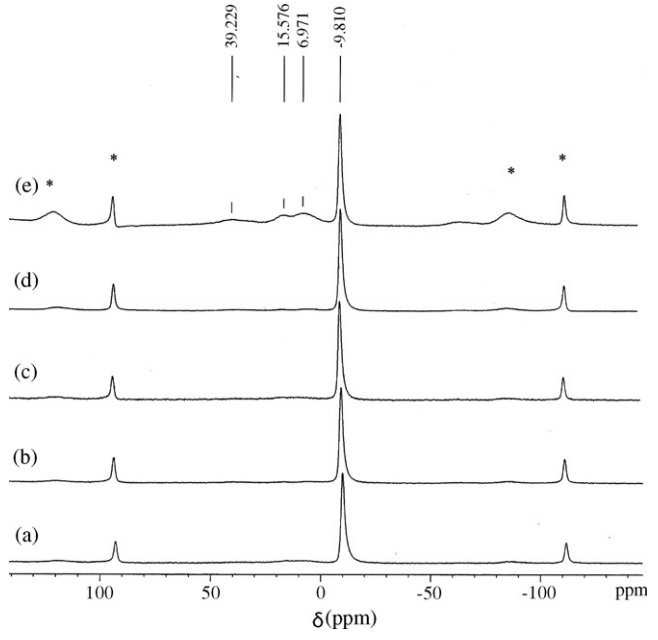


Fig. 7. $^{27}$Al NMR spectra of TCP–26.52 wt% Fap composites sintered at various temperatures and with different wt% $Al_2O_3$ for 1 h: (a) 2.5 wt% $Al_2O_3$, 1100 °C; (b) 2.5 wt% $Al_2O_3$, 1200 °C; (c) 2.5 wt% $Al_2O_3$, 1300 °C; (d) 2.5 wt% $Al_2O_3$, 1400 °C and (e) 10 wt% $Al_2O_3$, 1300 °C (*: rotation band).

The X-ray diffraction patterns of TCP–26.52 wt% Fap composites heated without and with $Al_2O_3$ at various temperatures for 1 h are reported in Fig. 8. The XRD patterns of samples sintered at 1100 °C, 1200 °C and 1300 °C with 2.5 wt% $Al_2O_3$ show the presence of Fap, β-TCP and $Al_2O_3$ traces (Fig. 8a–c). The XRD patterns of the samples sintered at 1400 °C with 2.5 wt% $Al_2O_3$ show in more the presence of α-TCP, $Ca_4(PO_4)_2O$ and $CaAl_2O_4$ phases (Fig. 8d). When sintered

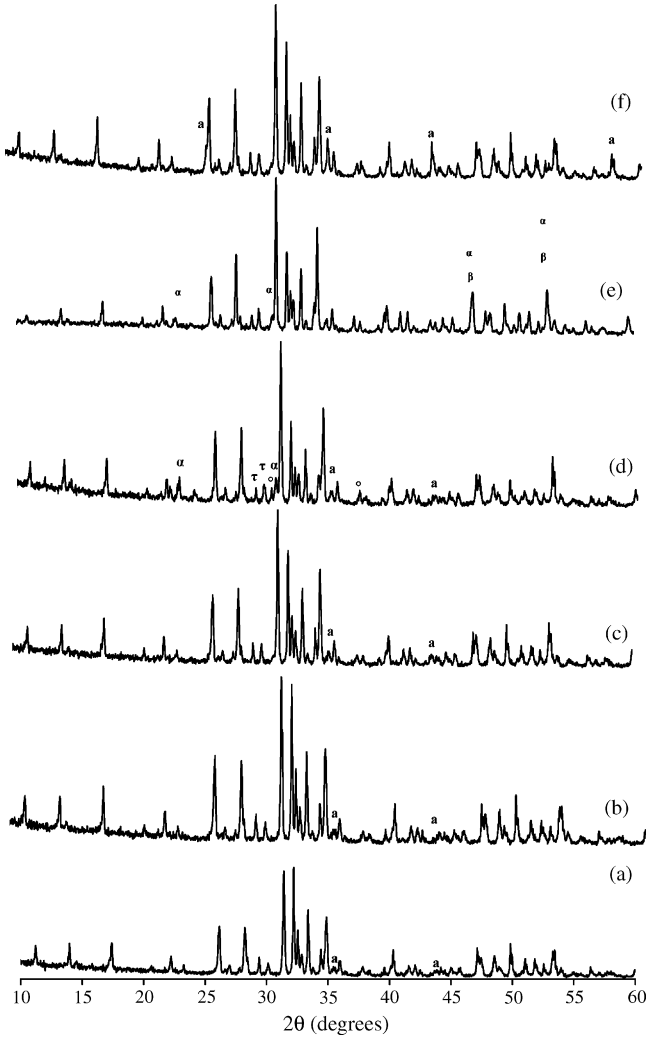


Fig. 8. XRD patterns of TCP–26.52 wt% Fap composites sintered with different wt% $Al_2O_3$ for 1 h at various temperatures: (a) 2.5 wt% $Al_2O_3$, 1100 °C; (b) 2.5 wt% $Al_2O_3$, 1200 °C; (c) 2.5 wt% $Al_2O_3$, 1300 °C; (d) 2.5 wt% $Al_2O_3$, 1400 °C; (e) 0 wt% $Al_2O_3$, 1300 °C and (f) 20 wt% $Al_2O_3$, 1300 °C (α: α-TCP; a: $Al_2O_3$; τ: $Ca_4(PO_4)_2O$; °: $CaAl_2O_4$; β: β-TCP).

at 1100 °C (Fig. 8a), the composite retained initial phases (β-TCP, Fap and $Al_2O_3$ traces). The intensive peak in the patterns is relative to Fap. This result is confirmed by $^{31}P$ and $^{27}Al$ MAS-NMR analysis. In more, the new quantity of Fap is obtained by solid reaction between TCP and $CaF_2$. In the composite fabricated at 1200 °C (Fig. 8b), the resulting phases were similar to the case at 1100 °C. However, when the sintering temperature increases to 1400 °C (Fig. 8d), the Fap peak relativity decreases, illustrating probably a pronounced partial decomposition of Fap to TCP. Moreover, the calcium aluminates phase $CaAl_2O_4$ was also produced, suggesting the diffusion of $Al^{3+}$ in Fap during the decomposition process. The partial decomposition of Fap in the presence of $Al_2O_3$ at 1400 °C is probably explained as follows:

$$Ca_{10}(PO_4)_6F_{2(s)} + Al_2O_{3(s)} + H_2O_{(g)} \leftrightarrow 3Ca_3(PO_4)_{2(s)} + CaAl_2O_{4(s)} + 2HF_{(g)} \quad (4)$$

The presence of $CaAl_2O_4$ is also probably produced by solid reaction between $Al_2O_3$ and CaO, which is explained as follows:

$$CaO_{(s)} + Al_2O_{3(s)} \rightarrow CaAl_2O_{4(s)} \quad (5)$$

CaO is produced by solid reaction between $CaF_2$ and $H_2O$ [9]. Ben Ayed et al. show when the gas atmosphere is not fittingly dried, hydroxyfluorapatite can be formed and hydrolysis of $CaF_2$, which can be expressed by the following equation [9]:

$$CaF_{2(s)} + H_2O_{(g)} \rightarrow CaO_{(s)} + 2HF_{(g)} \quad (6)$$

$$Ca_{10}(PO_4)_6F_{2(s)} + xH_2O_{(g)} \rightarrow Ca_{10}(PO_4)_6F_{2-x}(OH)_{x(s)} + xHF_{(g)} \quad (7)$$

The reason for this might be that $F^-$ ion react with the water in air or gas atmosphere at high temperatures and is accordingly replaced by $OH^-$ [9]. This result is observed by Adolfsson et al. [15]. In fact, they show that the apatite reacted with the moisture in the air and partly converted to hydroxyfluorapatite or oxyhydroxyapatite.

These subsequent reactions ((4) and (5)) are similar to the previous reported by Kim et al. on the Hap–$Al_2O_3$ composites with the addition of $CaF_2$ [16] and reported by Adolfsson et al. on the phase stability aspects of various apatite–aluminium oxide composites [15].

The XRD analysis of TCP–6.52 wt% Fap composites sintered at 1300 °C for 1 h with various mass percentages of $Al_2O_3$ (0 wt%, 2.5 wt% and 20 wt%) is presented in Fig. 8e, c and f. When sintered without alumina, the composite contained initial phases (β-TCP, Fap and α-TCP traces) (Fig. 8e). However, when the mass percentage of $Al_2O_3$ increased to 2.5 wt% and 20 wt%, the $Al_2O_3$ peaks were still observed (Fig. 8c and f).

Only the pure phases of aluminium oxide, Fap and TCP are detected in the XRD pattern of samples sintered with 2.5 wt% $Al_2O_3$ at temperature less than to 1300 °C (Fig. 8a–c). The XRD powder patterns of TCP–6.52 wt% Fap composites sintered with 2.5 wt% $Al_2O_3$ at 1400 °C or above (Fig. 8d), revealed the presence of $Ca_4(PO_4)_2O$, $CaAl_2O_4$ and TCP. Adolfsson et al. confirm these results [15]. Indeed, they show for the apatite sintered with alumina phase a decomposition of apatite to TCP and calcium aluminates ($CaAl_2O_4$).

The SEM examination of the fracture surface of the TCP–6.52 wt% Fap composites sintered with 2.5 wt% $Al_2O_3$ at various temperatures (1100 °C, 1200 °C, 1300 °C and 1400 °C) is reported in Fig. 9. The fracture surfaces clearly reveal a distinct difference in the sample microstructure. At 1100 °C,

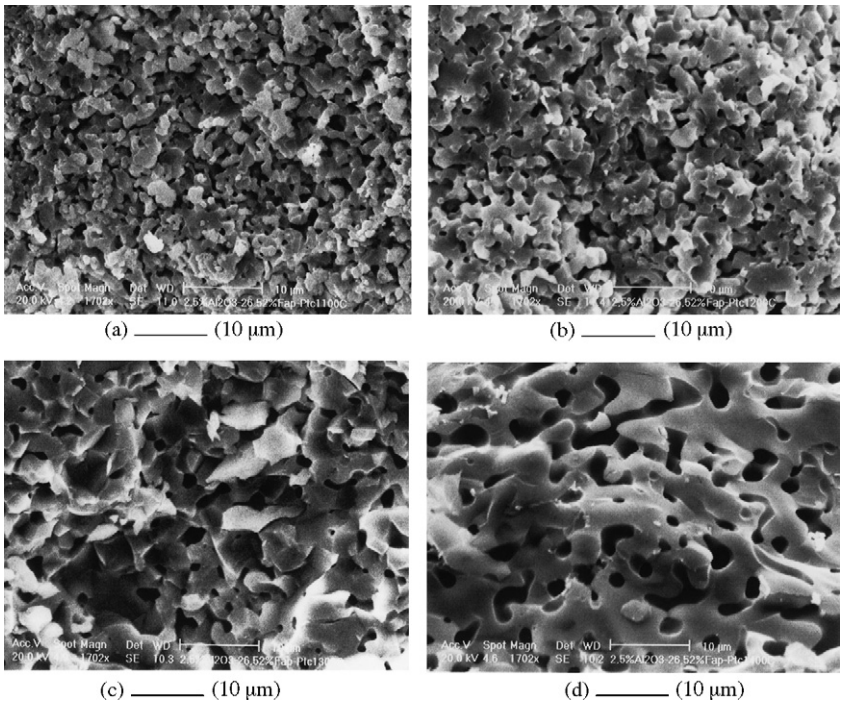


Fig. 9. SEM micrography of TCP–26.52 wt% Fap composites sintered with 2.5 wt% $Al_2O_3$ for 1 h at: (a) 1100 °C; (b) 1200 °C; (c) 1300 °C and (d) 1400 °C.

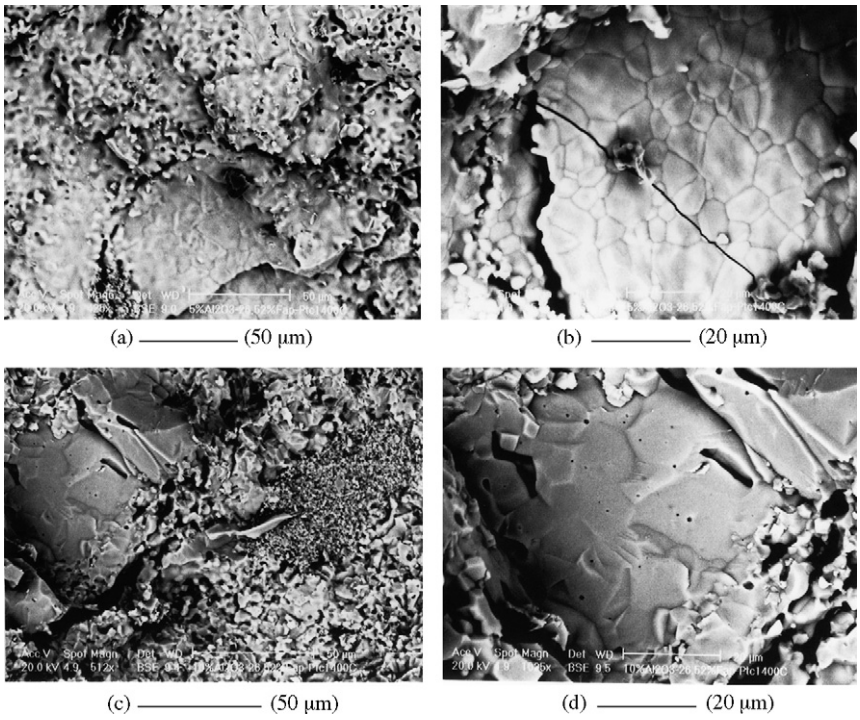


Fig. 10. SEM micrography of TCP–26.52 wt% Fap composites sintered at 1400 °C for 1 h with: (a) 5 wt% $Al_2O_3$; (b) 5 wt% $Al_2O_3$; (c) 10 wt% $Al_2O_3$ and (d) 10 wt% $Al_2O_3$.

the sample presents an important intergranular porosity which disappears partially when temperature increases (Fig. 9a–c). In the specimen sintered at 1200 °C, the grain has rounded appearance. DTA of Fap powder yielded an endothermic peak at about 1180 °C; which is attributed to the formation of liquid phase [8,9]. In this temperature range, the average grain size is about 2 μm at 1100 °C and 4 μm at 1300 °C. At this temperature (1300 °C), one notices a partials reduction of the porosity (Fig. 9c). At higher temperature (1400 °C), the composites densification is hindered by the formation of the large pores (Fig. 9d). Beside the grain growth, which becomes exaggerated at the highest temperatures; the microstructure exhibits an important intragranular porosity (Fig. 9d). The pore, which is roughly spherical, has a diameter varying approximately between 1 μm and 4 μm. Ben Ayed et al. also observed the formation of large pores at these temperatures, during the study of pressureless sintering of Fap [9]. They attributed it to the departure of volatile species produced by the hydrolysis of Fap and fluorite.

Fig. 10 shows the microstructural developments during the sintering of TCP–26.52 wt% Fap composites at 1400 °C for 1 h with various percentages of $Al_2O_3$ (5 wt% and 10 wt%), observed on fractured surfaces by SEM. The material firing at 1400 °C with 5 wt% and 10 wt% is constituted by two types of microstructure (Fig. 10a and c). This micrograph relative to composites sintered with 5 wt% $Al_2O_3$ reveals an important intragranular porosity and crack path in the composite (Fig. 10b). In specimen sintered with 10 wt% $Al_2O_3$, the microstructure is formed by continued surface, constituted by the two phases of calcium phosphate and small grain relative to $Al_2O_3$ additive (Fig. 10c). It should be noted that there are many cracks penetrating into the grain of TCP–26.52 wt% Fap composite (Fig. 10b and d). These cracks are caused by the allotropic phase transformation of TCP ($\beta \rightarrow \alpha$). This result is confirmed by Bian et al. [28].

## 4. Conclusions

The TCP–Fap composites present a good sinterability at 1300 °C, so an apparent porosity about 13% was reached without alumina. The biphasic calcium phosphate (TCP–Fap) has excellent biocompatibility and direct bond formation with the adjacent hard tissue. But its mechanical properties are generally inadequate for many load-carrying applications. These bioceramics have a low density which decreases the mechanical resistance. Alumina has been used in the TCP–Fap composites for its higher stability and its better densification and mechanical properties than TCP and Fap. So, $Al_2O_3$ additive was used for the TCP–26.52 wt% Fap composite densification. In fact, the apparent porosity for the TCP–26.52 wt% Fap composites with 2.5% is about 9%. At 1300 °C, XRD analysis of the composites reveals the presence of Fap and TCP without any other structures. This temperature was also used for densification of aluminium oxide–TCP–26.52 wt% Fap composites without any detectable phase changes. High temperatures (above 1300 °C) are not the best conditions for the composite densification. This is probably due to the formation of new compounds (α-TCP, $CaAl_2O_4$), illustrating a partially pronounced decomposition of Fap and the formation of a liquid phase which facilitates the phenomenon of diffusion. Thus, the density is influenced by these changes in microstructure and the formation of a large pore.

## References


[1] E.D. Franz, R. Telle, High Tech. Ceram. (1987) 31–41.
[2] L.L. Hench, Bioceramics: from concept to clinic, J. Am. Ceram. Soc. 74 (7) (1991) 1487–1510.
[3] F. Mark, P.W. Brown, J. Am. Ceram. Soc. 75 (12) (1992) 3401–3407.
[4] P. Uwe, E. Angela, R. Christian, J. Mater. Sci.: Mater. Med. 4 (3) (1993) 292–295.
[5] J.C. Elliott, Structure and Chemistry of the Apatite and Other Calcium Orthophosphates, Elsevier Science B.V., Amsterdam, 1994.
[6] E. Adolfsson, L. Hermansson, Biomaterials 20 (1999) 1263–1267.
[7] E. Landi, A. Tampieri, G. Celotti, S. Sprio, J. Eur. Ceram. Soc. 20 (2000) 2377–2387.
[8] F. Ben Ayed, J. Bouaziz, K. Bouzouita, J. Eur. Ceram. Soc. 20 (8) (2000) 1069–1076.
[9] F. Ben Ayed, J. Bouaziz, K. Bouzouita, J. Alloys Compounds 322 (1–2) (2001) 238–245.
[10] F. Ben Ayed, J. Bouaziz, I. Khattech, K. Bouzouita, Ann. Chim. Sci. Mat. 26 (6) (2001) 75–86.
[11] H.S. Ryn, H.J. Youn, K.S. Houng, B.S. Chang, C.K. Lee, S.S. Chung, Biomaterials 23 (2002) 909–914.
[12] A. Destainville, E. Champion, D. Bernache-Assolant, E. Labore, Matter. Chem. Phys. 80 (2003) 269–277.
[13] C.X. Wang, X. Zhou, M. Wang, Mater. Characterization 52 (2004) 301–307.
[14] F. Ben Ayed, J. Bouaziz, K. Bouzouita, Ann. Chim. Sci. Mater. 31 (4) (2006) 393–406.
[15] E. Adolfsson, L. Hermansson, J. Mater. Sci. 35 (2000) 5719–5723.
[16] H.W. Kim, Y.H. Koh, S.B. Seo, H.E. Kim, Mater. Sci. Eng. C 23 (2003) 515–521.
[17] F. Ben Ayed, J. Bouaziz, C.R. Physique 8 (2007) 101–108.
[18] E.C. Moreno, M. Kresak, R.T. Zahradnik, Nature 247 (1974) 64–65.
[19] J.F. Osborn, H. Neweslety, Biomaterials 1 (1980) 908.
[20] J. Huaxia, P.M. Marquis, J. Mater. Sci. 28 (1993) 1941–1945.
[21] Y.M. Kong, S. Kim, H.E. Kim, J. Am. Ceram. 82 (1999) 2963–2968.
[22] R. Ramachandra Rao, T.S. Kannan, Mater. Sci. Eng. C 20 (2002) 187–193.
[23] F. Ben Ayed, K. Chaari, J. Bouaziz, K. Bouzouita, C.R. Physique 7 (2006) 825–835.
[24] S. Brunauer, P.H. Emmet, J. Teller, J. Am. Chem. Soc. 60 (1938) 309.
[25] M. Yashima, A. Sakai, T. Kamiyama, A. Hoshikawa, J. Solid State Chem. 175 (2003) 272–277.
[26] L.S. Burrell, C.T. Johnston, D. Schulze, J. Klein, J.L. White, S.L. Hem, Vaccine 19 (2001) 275–281.
[27] B. Moreno, B. Bailey, S. Luo, M.B. Martin, M. Kuhlen Schmidt, S.N.J. Moreno, R. Docampand, E. Oledfield, Bio-chemical Biophys. Res. Commun. 284 (2001) 632–637.
[28] J.J. Bian, D.W. Kim, K.S. Hong, Mater. Lett. 58 (2004) 347–351.